https://doi.org/10.5194/egusphere-2024-2790
Preprint. Discussion started: 11 November 2024

Collision with Seamount Triggers Breakup of Antarctic Iceberg

Xianwei Wang[1, 2, 3*], G. Hilmar Gudmundsson[4] and David M. Holland[2, 5]

1. School of Oceanography, Shanghai Jiao Tong University, Shanghai, China
2. Center for Global Sea Level Change, New York University Abu Dhabi. Abu Dhabi, United Arab Emirates.
3. Key Laboratory of Polar Ecosystem and Climate Change (Shanghai Jiao Tong University), Ministry of Education, Shanghai 200030, China.
4. Department of Geography and Environmental Sciences, Northumbria University, Newcastle, UK.
5. Courant Institute of Mathematical Sciences, New York University. New York 10012, United States of America.

*Correspondence: xianwei.wang@sjtu.edu.cn

https://doi.org/10.5194/egusphere-2024-2790
Preprint. Discussion started: 11 November 2024

Abstract

Iceberg A68a calved from Larsen C ice shelf, experienced several major calving when drifting around the South Georgia Island in late 2020. Here, we show for the first time that the decisive factor for its calving was a collision with the surrounding seamount. By treating the iceberg as a deformable body in an established ice-flow model, we show how its collision with the seafloor created huge stresses within the iceberg that led to its disintegration. The drifting and rotating of the iceberg, while grounded, further enhanced its breakup. Moving over a grounded shoal increased the tensile stresses by a factor of almost one hundred more than immobile grounding alone, and rotational motion about the pinning point increased the stresses by another twenty percent. Modeling the fracture and breakup of a large tabular iceberg is an essential step toward better understanding the life cycle of an iceberg. The possible collapse of the marine-based sectors of the great ice sheets in a warming world may lead to a massive increase in the number of icebergs in the surrounding oceans. It will be crucial to be able to understand where such icebergs drift and how they ultimately disintegrate into the ocean.

Keywords: iceberg A68a; iceberg grounding and calving; calving modeling; the South Georgia Island;

https://doi.org/10.5194/egusphere-2024-2790
Preprint. Discussion started: 11 November 2024

1. Introduction

Tabular icebergs in the Southern Ocean are primarily calved from three large ice shelves in Antarctica: the Ross (Lazzara et al., 1999; Joughin and MacAyeal, 2005), Filchner-Ronne (Scambos et al., 2005), and Amery Ice Shelves (Fricker et al., 2005). In the last two decades, ice shelves in the Antarctic Peninsula have become more unstable and experienced rapid calving (Scambos et al., 2004; Rignot et al., 2004; McGrath et al., 2012). After calving from an ice shelf, an iceberg starts its journey through the Southern Ocean, along the way playing a significant role in sea-ice formation (Massom et al., 2001, 2018), polynya occurrence (Robinson & Williams, 2012), dense shelf water export (Williams et al., 2010), and ocean primary production (Arrigo et al., 2002; Arrigo & van Dijken, 2003). An iceberg may even affect penguin colonies when grounded on a continental shelf (Kooyman et al., 2007). Driven by wind forcing, ocean currents, and the Coriolis force (Gladstone et al., 2001; Wagner et al., 2017), Antarctic icebergs usually drift vast distances around the continental shelf, occasionally, drifting north and eventually melting into the surrounding ocean (Merino et al., 2016; Silva et al., 2006). During drift, tabular Icebergs survive rapid surface melting (Jansen et al., 2005), basal melting (Russell, 1980; Jansen et al., 2007; Braakmann-Folgmann et al., 2022), ocean wave rush (MacAyeal et al., 2006), and ocean current shear (Huth et al., 2022). Eventually, they break up and release smaller icebergs (Wagner et al., 2014), hurrying up their melting into the ocean. Breakup is a natural process for tabular icebergs drifting in the ocean, but the breakup mechanism of tabular icebergs has yet to be fully understood.

https://doi.org/10.5194/egusphere-2024-2790
Preprint. Discussion started: 11 November 2024

Rapid change and breakup of tabular icebergs in the Southern Ocean are frequently monitored by remote sensing satellites that observe lateral changes in areal extent (Stuart and Long, 2010; Scambos et al., 2005; Braakmann-Folgmann et al., 2022). Further combining altimetry measurements, vertical changes of tabular icebergs can be accurately quantified (Braakmann-Folgmann et al., 2022), providing important ancillary information to understand an iceberg breakup event. Breakup results from ice fracture and subsequent rift formation in response to stresses that cause crevasse propagation (Benn et al., 2007; Cuffey & Paterson, 2010; Alley et al. 2008). When stresses exerted on an iceberg exceed some threshold, fracture tends to occur and develop perpendicular to the maximum tensile stresses. As the highest frequency of remote sensing observation is at best daily, the rapid ice fracture and breakup process are difficult to capture by such. Because of a lack of observation data, studies have yet to be conducted to understand the breakup of tabular icebergs (Bouhier et al., 2018).

A calving event on the Larsen C Ice Shelf off the Antarctic Peninsula in July 2017 gave birth to one of the most enormous tabular icebergs ever recorded, named A68, with an area of almost ten percent of the ice shelf (Hogg & Gudmundsson, 2017). In early 2021, the main body of A68 (hereafter A68a) drifting in the Southern Ocean disintegrated and disappeared quickly in the ocean. Before its rapid vanish, several major breakup occurred (Braakmann-Folgmann et al., 2022) which may have played important role in its rapid disappearance. When drifting in the ocean, two major breakup of A68a when A68a drifting away from the South Georgia Island was attributed to the large shear forces caused by differences in ocean currents (Huth et al., 2022). When A68a melting

https://doi.org/10.5194/egusphere-2024-2790
Preprint. Discussion started: 11 November 2024

in the ocean, it cooled down and diluted the surrounding ocean water (Smith and Bigg. 2023), causing deepening of the underlying water mass (Tarling et al. 2024), having significant influence on the surrounding marine ecosystem. However, the first breakup when A68a drifting close to the South Georgia Island was not fully understood, but likely to be caused by collision with seafloor (Huth et al., 2022). More investigation and evidence is required to better understand this breakup as this collision may have weaken the iceberg, causing its rapid melting into the surrounding ocean.

This research uses available multi-source remote sensing data to investigate the breakup of A68a when it drifted close to the South Georgia Island in the Southern Ocean. We begin by revealing its grounding status through remote sensing data. Then, we turn to an established ice-flow model to calculate the tensile stresses exerted on the iceberg under various drift scenarios while grounded. We uncover the breakup mechanism of the large tabular iceberg A68a due to its interaction with seafloor shoals on its drift across the Southern Ocean.

2. Data

We use Sentinel-1A/B Extra Swath GRD data from July 2017 to February 2021 and MODIS image from December 2020 to May 2021 (Fig. 1, 2, Table S1 and S2) to observe the major breakup, drifting trajectory, and boundary changes of A68a. Iceberg location from July 2017 to July 2019 from Brigham Young University (BYU) Microwave Earth Remote Sensing (MERS) Antarctic Iceberg Tracking Database (Budge and Long, 2018) is used to show part of the drifting trajectory of A68a (Fig. 3). Five tracks of

https://doi.org/10.5194/egusphere-2024-2790
Preprint. Discussion started: 11 November 2024

Cryosat-2 Synthetic Aperture Radar (SAR) Geophysical Data Record (GDR) data during November 1 to December 16, 2020 are used to extract the freeboard of A68a (Fig. 4). The freeboard data were used to invert ice thickness by using firn air thickness data (Holland et al., 2011). Seafloor Bathymetry data from the General Bathymetric Chart of the Oceans (GEBCO) is used to investigate the grounding section of A68a (Fig 3b). Tide height data from CATS2008 (Padman et al. 2002) is used to investigate sea surface changes in the vicinity of A68a. ERA-5 data from December 2020 from ECMWF are used to analyze wind speed and direction change, and pressure change near the sea surface around A68a. Monthly averaged ocean current data from Circulation and Climate of the Ocean (ECCO) V4r4 data from every December during 1992-2017 is used to characterize the upper ocean currents around A68a.

Insert Figure 1 here

Insert Figure 2 here

3. Method

In this study, we use remote sensing images to detect area, drifting trajectory, drifting and rotating speed of iceberg A68a first, and then use satellite altimetry to detect freeboard, invert thickness of A68a when the iceberg drifted close to the South Georgia Island. The mass of A68a before breaking up was predicted and the rift line where A68a calved along was extracted. Grounding status was detected using thickness and seafloor bathymetry data. Finally, using all parameters extracted above, Ua model was

https://doi.org/10.5194/egusphere-2024-2790
Preprint. Discussion started: 11 November 2024

set to investigate the deviatoric stresses exerted on iceberg A68a. The methods for all the processing are described as follows.

3.1 Drifting Trajectory and Area Changes of Iceberg A68a

Part of the drifting trajectory of A68a from the Antarctic Iceberg Tracking Database until July 2019 is shown in Fig. 3a. Using Sentinel-1A/B GRD and MODIS data, the boundaries of iceberg A68a at different observation dates are extracted by human interpretation (Wang et al. 2016) using ArcGIS, and multiple polygon shapefiles are generated. Then, the centroid locations of all shapefiles are calculated using the Geometry Calculator with ArcGIS. Finally, the drifting trajectory of iceberg A68a between July 2017 and April 16, 2021, is generated using these centroid locations (black star in Fig. 3a). In Fig 3a, the red (A68 iceberg) and the grey (A68a iceberg) circle points are obtained from the Antarctic Iceberg Tracking Database (Budge & Long, 2018) . The black star points (A68a) are extracted from Sentinel-1 and MODIS satellites (Supp. Material). The observation dates of the A68a position are formatted as 'yyyymmdd' and illustrated in black. AP stands for Antarctic Peninsula. The grounding line of the Antarctic Ice Sheet is marked with a blue curve. The background is topography (Arndt et al. 2013), including the Antarctic Peninsula, South Georgia Island, and intervening the seafloor.

Insert Figure 3 here

https://doi.org/10.5194/egusphere-2024-2790
Preprint. Discussion started: 11 November 2024

The outline, calving progress of A68a when drifting close to the South Georgia Island is shown in Fig 3b. The background in Fig. 3b is the topography in and around South Georgia Island (Lambert azimuthal equal-area projection). The inset in the upper right of Fig. 3b is a zoom-in of the region indicated with a black square box in the panel, revealing a seamount feature. It shows a seafloor shoal (symbolized by the letter S) with bathymetry increasing from -250 m to close to sea level at a peak (symbolized by the letter P). The isobaths from -250 to 0 are drawn with an interval of 50 m.

The boundary polygon shapefiles extracted from remote sensing images are projected to an equal area projection (Lambert Azimuthal Equal Area) using ArcGIS and the area change of A68a is fitted with the least square method (Fig. 3c). The areas of derivative icebergs A68b, A68c, A68d, A68e, A68f, and A68g during several major breakup events are indicated with color circles. The accelerating areal-losing rates for three distinct periods (referred to as the first, second, and third phases of the iceberg's journey) are illustrated with grey line segments and the rates specified in km^2/a.

3.2 Drifting and Rotating Speed of Iceberg A68a

The centroid location and the time interval of both observations of A68a are used to calculate the drifting velocity, assuming a linear drift of A68a. The drifting velocity of iceberg A68a is obtained by dividing the time interval with drifting distance. Besides drifting, A68a also rotated in a clockwise direction (Fig. 3b). It is assumed iceberg A68a rotated around the center of mass (centroid). The rotating velocity is obtained by following two steps: (1): centroid normalization, and (2): rotation angle extraction.

Centroid normalization is first conducted to make sure both boundary files have (0, 0) as

https://doi.org/10.5194/egusphere-2024-2790
Preprint. Discussion started: 11 November 2024

their centroid. Rotation angle calculation is decided by how many degrees are required to be rotated until the best match of both outlines is found. Then the angular velocity of iceberg A68a is calculated by dividing the drifting period with rotation angle.

3.3 Freeboard of Iceberg A68a before Breakup

Cryosat-2 measurements less than 55 m (Holland et al. 2011) over A68a can be identified virtually from five different tracks in Fig. 4 (A68a is the only large iceberg that appeared in this region). Following the method from Wang et al. (2016), the sea surface height and top of the iceberg are determined for each track, and mean freeboard of A68a from each track of Cryosat-2 is calculated by Eqn. 1.

$$F_i = E_i - S_i \quad (1)$$

$$F = \frac{1}{5}\sum_{i=1}^{5} F_i \quad (2)$$

where E_i, S_i and F_i indicates the ice surface height, sea surface height and mean freeboard of iceberg A68a from track i of Cryosat-2.

We assume iceberg A68a has a uniform freeboard here. The final freeboard of A68a, which is 32.5± 1.0 m (1.0 m as the standard deviation of freeboard, Table S3) is calculated as the mean of all the five freeboards estimated (Eqn. 2). *F* indicates the mean freeboard of the iceberg A68a.

Insert Figure 4 here

3.4 Rift Line Extraction of Iceberg A68a

https://doi.org/10.5194/egusphere-2024-2790
Preprint. Discussion started: 11 November 2024

MODIS observation on December 16, 2020 (Fig. 2e), was contaminated by clouds and not used to extract the outline of A68a. However, the A68a outline extracted from Sentinel-1A images (December 15, 2020) was shifted and rotated to match A68a shown in MODIS observation using the method introduced above. In this way the outline of A68a corresponding to MODIS observation time on December 16, 2020, is extracted. The Sentinel-1A image on December 15 was georeferenced to MODIS observation time using 17 Ground Control Points (Table S4, Fig. 2e). The georeferencing reached an accuracy of 36.1 m.

In the same way, the outline of A68a extracted from Sentinel-1 image on December 21, 2020, is shifted and rotated back to position on MODIS observation time, December 16, 2020, by using 11 Ground Control Points (Table S5). The georeferencing reached an accuracy of 5.8 m. One rift line is extracted by comparing two different boundaries of A68a before and after the breakup (Fig 5 and 6a).

Image of A68d from Sentinel-1 on December 21, 2020, was georeferenced to MODIS observation time using five Ground Control Points (Table S6). The georeferencing reached an accuracy of 51.6 m. In this way, another rift line is extracted (Fig 5 and 6a).

Insert Figure 5 here

3.5 Thickness and Draft of Iceberg A68a before Breakup

The firn layer thickness must be considered to invert ice thickness but is seldom known as no simultaneous measurement of the iceberg A68a is available. However, the firn air content of Larsen C ice shelf varied from 8.0 to18.0 m at the calving front (Holland et al.

https://doi.org/10.5194/egusphere-2024-2790
Preprint. Discussion started: 11 November 2024

2011). The firn layer on the surface of iceberg A68a may change due to surface snow accumulation, melt and refreezing process during its drifting to the north. However, it is difficult to calculate the firn air content because of lacking in-situ observation data. In this study, a mean air content of 13.0 m of iceberg A68a is assumed since A68a calved off Larsen C ice shelf and we neglect the firn air content change after the calving of A68a. Meanwhile, we give 2 m uncertainty for this approximation. Finally, the ice thickness of A68a is inverted assuming hydrostatic equilibrium, Eqns. (3) and (4).

$$\rho_w(T-F)=\rho_i I+\rho_a A \quad (3)$$

$$T=I+A \quad (4)$$

where ρ_w = 1028.0 kg m^{-3}, ρ_i = 918.0 kg m^{-3}, and ρ_a = 2.0 kg m^{-3}are densities of seawater, pure ice, and englacial air respectively (taken from Holland et al. 2011). *T, I* and *A* is the thickness of the iceberg, pure ice, and air layer respectively (in this study, *A*=13.0±2.0 m).

In this way, the thickness of iceberg A68a is inverted using Eqns. (3) and (4), which is 195.5 ± 19.1 m, and the ice draft is 163.0 ± 19.1 m.

The uncertainty of ice thickness inversion is calculated with Eqn. (5)

$$d_T=\frac{\rho_a-\rho_i}{(\rho_w-\rho_i)}d_A+\frac{\rho_w}{(\rho_w-\rho_i)}d_F \quad (5)$$

where d_A and d_F are the uncertainty of air layer thickness and freeboard of A68a, respectively.

3.6 Mass of Iceberg A68a before Breakup

Before the breakup, the area of A68a was close to 3825±89.0 km^2 (December 15, 2020). When taking 195.5±19.1 m as the average thickness of A68a which includes

https://doi.org/10.5194/egusphere-2024-2790
Preprint. Discussion started: 11 November 2024

13.0±2.0 m meter firn air and 182.5±19.2 m pure ice and using the ice and air density in Eqn. (3), the total mass of iceberg A68a was 642.2±69.0 Gt (1Gt=10^9 t).

3.7 Grounding Detection of Iceberg A68a

The method for grounding detection introduced by Wang et al. (2016) is adopted in this study. It is also assumed that the iceberg is floating first, and compare the ice draft inverted from the freeboard with seafloor topography. The region with ice draft lower than seafloor bathymetry indicates grounding (negative comparison result in Fig. 6b-c). A large negative value indicates a heavily grounding section of an iceberg. This process is performed by following Eqns. (6) and (7)

$$D = E_d - E_b \quad (6)$$

$$E_d = T - F \quad (7)$$

E_d and E_b are the elevations of ice draft and seafloor bathymetry respectively. *D* is the elevation difference of ice drift and seafloor bathymetry.

Insert Figure 6 here

3.8 Ua modeling Setting of Iceberg A68a collision with Seamount

Ice tends to fracture under critical tensile stresses forming rifts along which ice breakup occurs. In this study, a 2d shallow-ice-shelf approximation glacier model *Ua* (Gudmundsson. 2008, 2012, 2013) is employed to investigate the deviatoric stresses when iceberg A68a interacts with seafloor shoals. Because A68a was drifting and

https://doi.org/10.5194/egusphere-2024-2790
Preprint. Discussion started: 11 November 2024

rotating before colliding with the sea mountain, the drifting and angular velocity of A68a must be inverted first by exerting an appropriate drag force on the iceberg in *Ua*.

Since the drifting of large icebergs (length>10 km) is primarily affected by ocean currents (Wagner et al. 2017), it is assumed that the drifting and rotating of A68a was a consequence of ocean currents only. In *Ua*, the ocean drag term is applied by following Eqn. (8)

$$t = (1-\mathcal{G})C_o^{-\frac{1}{m_o}}(v_b - v_o)^{\frac{1}{m_o}-1}\overrightarrow{(v_b - v_o)} \qquad (8)$$

where t stands for ocean drag, $\mathcal{G}$ floating/grounding mask of the iceberg. The drag coefficient is indicated with $C_o^{-\frac{1}{m_o}}$, where v_o and v_b stand for ocean current and basal ice velocity, respectively.

In Ua, the freeboard and thickness extracted from Section 3.3 and 3.5 was used to configure the surface (32.5 m) and bottom (-163.0 m) elevation of iceberg A68a. The seafloor bathymetry was input to set the lower boundary for ice-seafloor interaction modeling. The temperature of iceberg was set as -20 °C. The parameter A and n in Glen flow law was set as 2.9377×10^{-9} and 3 respectively. Surface and basal mass balance of the iceberg when interacting with the seafloor was set as 0 and neglected. Since the drifting of large icebergs (i.e., length >10 km) is primarily affected by ocean currents (Wagner et al. 2017), an appropriate ocean drag parameterization is of critical importance in *Ua*. The ocean drag coefficient C_0 was set as 0.4×10^4 (See section 5.1 for more details of this setting). A tuning choice reproduces the observed drifting and rotation speed of A68a before seamount impact. The drifting velocity of the iceberg in x

https://doi.org/10.5194/egusphere-2024-2790
Preprint. Discussion started: 11 November 2024

and y direction was set as 24.5 cm/s and -3.0 cm/s respectively. The rotational velocity of the iceberg was set as 15.1°/d. It allows investigation of the deviatoric stresses exerted on the iceberg during seamount grounding. It implicitly assumes that the iceberg is rigid during the simulated seamount interaction. No calving law is applied. The air drag was not considered in the ice-seafloor interaction modeling. Detailed setting of ice-seafloor interaction modeling in Ua can be found from Table 1.

Insert Table 1 here

4. Results

4.1 Life History of A68a

After the birth of A68a, it drifted north and finally disappeared in the Southern Ocean in May 2021 (Fig. 3, 2a-2d). The drifting trajectory and areal changes of A68a from remote sensing (Fig. 3a, 3c) indicate that iceberg A68a has lasted almost four years, from July 2017 to May 2021. The maximum latitude A68a reached was 52 °S (Fig. 3a, and Fig. 2a-2d). A68a experienced six major breakup events (Fig. 1). The total areal ice loss in generating nascent icebergs during these breakups was > 2000 km^2 (Fig. 3c), more than a third of the original iceberg A68a. This suggests that the decimation of a large tabular iceberg in Antarctica occurs through a sequence of breakups.

The lifespan of A68a shows three different areal-losing rates (Fig. 3c) during its evolution, which are -156 km^2/a, -1204 km^2/a, and -11,990 km^2/a, sequentially. The increasing areal-losing rates demarcate three distinct evolutionary periods of this well-

https://doi.org/10.5194/egusphere-2024-2790
Preprint. Discussion started: 11 November 2024

documented, large tabular iceberg adrift in the Southern Ocean. The ratio of areal-losing rates for three different phases is approximately 1:8:80, which signals that once an iceberg has arrived at the third phase, it is well on its way to rapidly vanishing into the surrounding ocean. The survival time ratios of 6:2:1 and total ice loss ratios of 1:3:11 of the three different phases combine to indicate that the rate and volume of ice loss of the A68a iceberg accelerate over time.

A major breakup event ensued when A68a eventually drifted to South Georgia Island, and A68a gave birth to another iceberg, A68d (Fig. 1c, and 3b). Moderate Resolution Imaging Spectroradiometer (MODIS) data show that the breakup event occurred on December 16-17, 2020 (Fig 2e, 2f). Sentinel-1A/B synthetic aperture radar data reveals that after the breakup, A68a decreased to ~3582±8 km^{2,} and the area of A68d was 147±1 km^{2} (Fig. 3c). Using satellite observations from MODIS, Sentinel-1A/B, and adding in Cryosat-2 radar altimeter data (Fig. 4) the bulk properties of A68a were established during December 15-16, 2020. At that moment, it was ~195±19 m thick, weighed some ~642±69 Gt, drifted at a speed of 24±2 cm/s, and rotated with an angular velocity of ~15±2°/d, clockwise. Furthermore, the drifting speed during the previous two days, December 15-16, 2020, did not change much from the days preceding them, December 13-15, 2020 (Table. S7). This indicates the sizeable tabular iceberg had large inertia to sustain a relatively constant motion.

4.2 Seafloor Grounding

https://doi.org/10.5194/egusphere-2024-2790
Preprint. Discussion started: 11 November 2024

Bathymetric data illustrates that in the vicinity of South Georgia Island, there is a seamount with a subsea elevation rising from about -250 m to the surface (Fig. 3b, 6a). MODIS geospatial data (Fig. 2e, 6a) shows that A68a hovered over part of the seamount on December 16, 2020. The grounding status of A68a at this juncture in time has been assessed by assuming hydrostatic equilibrium, employing firn-layer thickness (Holland et al. 2011) and ice thickness inverted from remote sensing. The result indicates > 3 km^2 of the iceberg (18 pixels) was grounded on the seamount (Fig. 6b and 6c). At its most severely grounded point, the iceberg was estimated to be lifted about 30 m out of floatation. Grounding on the seamount resulted in a sudden basal drag on the rapidly drifting and rotating iceberg. A seafloor drag's abrupt appearance dramatically altered the dominant balance of forces of the wind and currents and the iceberg's internal stresses.

To visualize the rift along which A68a calved during December 16-17, 2020, boundary outlines of A68a and A68d, extracted from Sentinel-1A on December 21, are georeferenced to MODIS data on December 16 by matching ground control points (Fig 5d and 5e). The georeferenced icebergs reflect two rifts (named Rift 1, Rift2) on December 16 (Fig. 5e and 6a). During the breakup event, a region formed between the two rifts, and about 2 $km^{2,}$ was lost. The timing of the breakup, as seen from remote sensing, suggests this modest loss was a contributing factor in the more significant breakup. Coincidently, analysis reveals that Rift 1 was overlaying the most severely grounded region (Fig. 6a and 6e), which suggests that the area is critical to the breakup of A68a.

https://doi.org/10.5194/egusphere-2024-2790
Preprint. Discussion started: 11 November 2024

4.3 Maximum Tensile Stress for Iceberg-Seafloor Interactions

Using the standard *Ua* parameter settings (Table. 1), the basal ice speed, ice surface elevation, and deviatoric stresses exerted on A68a are simulated in Fig. 7a-d. Examining rifts extracted from remote sensing, the maximum surface elevation of A68a is observed to be located on Rift 1. Furthermore, the simulation indicates that the maximum tensile stresses appear over grounded regions, and the location of maximum tensile stresses is on Rift 1 (within <200 m, Fig. 7b-c). The rift observed from remote sensing crosses the simulated location of maximum tensile stresses exerted on iceberg A68a which support the theory from (Benn et al. 2007) that the tensile cracks tend to occur perpendicular to the maximum tensile stresses.

Insert Figure 7 here

5. Discussion

5.1 Ocean Drag Coefficient in Ua

The drag coefficient is set differently for iceberg and sea-ice studies (Bigg et al 1997; Flato & Hibler 1992). Since *Ua* is a two-dimension glacier model and external forces exerted on the sidewall of an iceberg are not considered, we assume an iceberg is a thick piece of sea ice and only consider the basal drag applied to the iceberg in this study. Flato and Hibler (1992) suggested the ocean drag coefficient was 0.0055 and the ocean drag was quadratic to ocean current velocity, from which one can get the following settings: $m_o = 0.5$, C_o=0.4 (unit: $\sqrt{(\mathrm{m/s})/\mathrm{Pa}}$).

Without considering the ocean drag force, the basal ice velocity and deviatoric stresses of A68a from diagnostic runs is shown in Fig. 8a and 8e. Uniform deviatoric stresses are shown inside of the iceberg and no abnormally large stresses occur at the boundary of A68a. However, after applying ocean drags and zero ocean currents in *Ua*, enlarged deviatoric stresses are found at boundary nodes when the ocean current is set as zero (Fig. 8b-8d, 8f-8h). This result indicates that the setting about C_o=0.4 is not appropriate because no significant drag at the boundary would occur when putting an iceberg in a still ocean. The variation of maximum deviatoric tensile stresses exerted on A68a is shown in Fig. 8 when is set to various values.

Insert Figure 8 here

Without more observation data related to iceberg drifting, it is difficult to determine the values of C_o accurately. However, Fig. 8i indicate that smaller setting of C_o leads to larger stresses ocean drag exerted iceberg and larger tensile stresses at the boundary of the iceberg. When C_o >0.4×10^4, the maximum tensile stresses exerted on A68a in the still ocean is approaching that from diagnostic runs without applying ocean drags. Based on this, C_o=0.4×10^4 is assessed as an appropriate setting since neither significant direction change of deviatoric forces occurred inside of the iceberg A68a, nor large tensile stresses at the boundary.

5.2 Relation of Maximum Tensile Stress With Grounding, Drifting and Rotating Status

The *Ua* glacier model is used to investigate further the relationship of maximum tensile stresses to grounding, drifting, and rotation of A68a. As a sensitivity experiment, the model seamount is lowered by 50 m so that iceberg A68a experiences no drag in the vicinity of the seamount. Tensile stresses no more significant than 0.1 MPa are simulated inside the iceberg (Fig. 9). In the next experiment, restoring the seamount to its observed height, with A68a drifting with a speed consistent with observations from remote sensing but with no rotation, the maximum tensile stress jumps to 9 MPa over the grounding region (Fig. 7d). An increase of almost a factor of one hundred. When further incorporating the rotation of A68a, the maximum tensile stress increases to 10 MPa (Fig. 7d), a further twenty percent increase. These sensitivity experiments demonstrate that grounding a rapidly drifting and rotating iceberg on a seafloor shoal leads to significant tensile stresses inside the iceberg. Since icebergs tend to fracture under significant tensile stresses, and the rifts from remote sensing and maximum tensile stresses from glacier modeling coincide, it is concluded that substantial tensile stresses associated with grounding triggered the breakup of A68a.

Insert Figure 9 here

Modeling results indicate that grounding only A68a on the seamount, with no motion, would generate maximum tensile stress < 0.2 MPa, even considering seafloor changes by ±20 m. However, the maximum tensile stress increases to about seventy times when additionally applying half of the drifting speed observed from remote sensing, reaching eighty times than grounding only when full drifting speed is simulated. Simulations

https://doi.org/10.5194/egusphere-2024-2790
Preprint. Discussion started: 11 November 2024

suggested that larger tensile stresses could occur in A68a when further raising the seafloor, thus simulating more severe grounding. When lowering the seafloor by 20 m (other settings the same as Table 1), the maximum tensile stress was about 6.0 MPa. When raising the seafloor by 20 m, the maximum tensile stresses experienced by A68a increased to > 20 MPa. This confirms that grounding an iceberg with a considerable drifting speed generates significant tensile stresses inside the grounded section of the iceberg. Less obvious, perhaps, more severe grounding non-linearly increases the maximum tensile stresses.

The rotation of the iceberg is another factor influencing the maximum tensile stresses. When iceberg A68a is simulated to rotate as observed by remote sensing data (15.1°/d, clockwise direction, other settings the same as Table 1), a maximum tensile stress > 10 MPa appears over the grounding region of A68a. Modeling results indicate that for the same seafloor bathymetry, more significant angular velocity exerts more considerable tensile stresses on A68a. Using all data from different grounding statuses of A68a, the maximum tensile stresses increase by about 10, 20, and 30 percent when additional angular velocity at 8 °/d, 15°/d, and 23°/d are applied. In short, rotation enlarged the maximum tensile stresses experienced in A68a by about twenty percent, contributing to the breakup during December 16-17, 2020.

5.3 How Polar Cyclone and Ocean Tide Contributing to Breakup of A68a

As mentioned, the drifting of large tabular icebergs (>10 km) is primarily driven by ocean currents (Wagner et al. 2017). The currents derived from monthly averaged (December) ECCO V4r4 data (Wunsch et al. 2009) over the region of A68a is shown in Fig 10a. Historical ocean current data indicate a constant eastward flow (Fig. 10a and Supp. Animation 1), which can help to explain the primary eastward drifting of A68a towards the seamount. The average of 10-meter U and V wind components from ERA5 (Hersbach et al. 2020) during December 1-16, 2020 over A68a, which was captured by MODIS at 12:45 UTC on December 16 (white polygon) in shown in Fig.10b. The average west wind extracted from the reanalysis data, supports the eastward drifting A68a. When A68a drifts to the vicinity of South Georgia Island, sea surface changes associated with atmospheric pressure changes and ocean tide could alter the interaction of A68a with the seamount, effectively lifting the iceberg over the seamount to some extent.

Insert Figure 10 here

The tide height changes during December 15-17 from CATS2008 (Padman et al. 2002) (Fig. 10e) indicate that the sea surface height change caused by the tide around iceberg A68a reached > 1 m. The surface elevation change by tides may facilitate A68a to reach higher seafloor shoals during high tide and further cause iceberg A68a to be grounded more during low tide when it is lowered and dropped back onto the shoals. ERA5 data show that during December 15-17, 2020, a polar cyclone passed by A68a (Fig. 10c-d, and Supp. Animation 2-3). The pressure in Fig. 10e is calculated by

https://doi.org/10.5194/egusphere-2024-2790
Preprint. Discussion started: 11 November 2024

averaging over the region from Latitude: -55° to -56°, to longitude: -37.25° to -37.75° (iceberg location seen in Fig. 10b) and is indicated with blue curves. This region's standard deviation of pressure is used as the error bar. When the polar cyclone moved close to A68a, the mean sea level pressure dropped about 30 hPa (Fig. 10e), which could significantly raise the sea surface by approximately 0.3 m (Fig. 10f) and facilitate A68a climbing up to a higher region of the seamount.

Fig. 10e also show the tidal height predictions derived from the tide model CATS2008. The curves marked with asterisks and circles show the tide-height prediction from the northern (37.371° W, 54.979° S) and southern (37.548° W, 56.106° S) tips of A68a, respectively. The red star indicates the minimum tidal height at the major breakup event. Fig. 10f shows the total sea surface change from tide and cyclone effects. Before MODIS observation on December 16, a peak sea surface elevation occurs, one can assist A68a in a climb up to the most elevated location on the seamount. After the MODIS observation, the most significant sea surface drop occurred almost a day later (Fig. 10e, f), when A68a would ground most severely on the seamount, effectively shipwrecked. The red star indicates the minimum sea surface from pressure and tide changes at the major breakup event. The vertical blue, red, and green dashed lines in Fig. 10e, and f give the observation time of the Sentinel-1 image on December 15, and MODIS observation on December 16 and 17, respectively. Since larger tensile stresses tend to occur at more severe grounding icebergs, iceberg A68a most likely broke up at that time (17:00 UTC on December 16).

https://doi.org/10.5194/egusphere-2024-2790
Preprint. Discussion started: 11 November 2024

6. Conclusion

Large tabular icebergs experience breakup while drifting in the ocean, ultimately melting and vanishing into the ocean, the destiny of all icebergs. The breakup generates many smaller icebergs and increases the area for iceberg-ocean interaction, speeding up the iceberg melting. Seafloor shoals, such as a seamount, lead to iceberg grounding and are a barrier to iceberg drift. When an iceberg drifts toward a seafloor shoal with a relatively large speed, if the seafloor is higher than the iceberg draft, a grounding event occurs, even despite an iceberg having a large mass and inertia to maintain its speed. Grounding of rapidly drifting and rotating icebergs tends to create significant deviatoric stresses inside an iceberg, which may trigger the formation of rifts and facilitate iceberg breakup.

For an iceberg that drifts towards a seafloor shoal, the sea surface change caused by a rising tide and weather events, such as a polar cyclone, may make the iceberg drift to a higher region of the seafloor shoal. After the passing of a polar cyclone and during low tide, a follow-on significant sea surface drop can make iceberg grounding more severe on the seafloor shoal, generating even more enormous tensile stresses in the iceberg and facilitating the breakup of the iceberg across the maximum tensile stress point.

The later, rapid vanishing of iceberg A68a into the ocean is fully explained by the breakup event that occurred on December 16, 2020, caused by the collision of A68a with a seamount. We demonstrate the first successful case of using a large tabular iceberg as a natural laboratory, with remote sensing observations as a data source and

https://doi.org/10.5194/egusphere-2024-2790
Preprint. Discussion started: 11 November 2024

a glacier model as a tool to investigate iceberg calving, expanding glacier-seafloor interaction research. Looking to the future, the possibility of a collapse of the marine-based-portions of the great ice sheets has been raised. The concomitant rapid dispersal of numerous icebergs into the ocean would influence local ocean circulation and local atmosphere temperature by providing freshwater input into the ocean surface, affecting the ocean-mixed layer regime, vertical convection, and the surface albedo. As demonstrated in this study, understanding the trajectory of such icebergs and their breakup mechanism will contribute to better forecasting an iceberg's fate and the state of the polar oceans.

https://doi.org/10.5194/egusphere-2024-2790
Preprint. Discussion started: 11 November 2024

Acknowledgments

X.W. was supported by the National Natural Science Foundation of China (grant 42276237), the Oceanic Interdisciplinary Program of Shanghai Jiao Tong University (grant SL2022PT205) and the Shanghai Frontiers Science Center of Polar Science (SCOPS). D.M.H. was supported by the Center for global Sea Level Change (CSLC) of New York University Abu Dhabi Research Institute (grant G1204), and the National Science Foundation (grants PLR-1739003, PLR-2151295) of the USA. We thank Won Sang Lee and Alex Fraser for their advice and helpful discussion on iceberg calving.

https://doi.org/10.5194/egusphere-2024-2790
Preprint. Discussion started: 11 November 2024

Data availability

Sentinel-1A/B data are downloaded from Copernicus Open Access Hub (https://scihub.copernicus.eu/). MODIS data are downloaded from Level-1 and Atmosphere Archive & Distribution System Distributed Active Archive Center (https://ladsweb.modaps.eosdis.nasa.gov/missions-and-measurements/modis/). Cryosat-2 GRD data are downloaded from Earth Online, European Space Agency (https://earth.esa.int/eogateway/catalog/cryosat-products). Seafloor Bathymetry data are obtained from the General Bathymetric Chart of the Oceans (GEBCO) (doi:10.5285/a29c5465-b138-234d-e053-6c86abc040b9) . The trajectory of A68a from 2017 to July 2019 is downloaded from The Antarctic Iceberg Tracking Database (https://www.scp.byu.edu/iceberg/). CATS2008 model is obtained from Earth & Space Research (https://www.esr.org/research/polar-tide-models/list-of-polar-tide-models/cats2008/). ERA5 data are obtained from ECMWF (https://www.ecmwf.int/en/forecasts/datasets/reanalysis-datasets/era5). ECCO V4r4 monthly averaged ocean current data are obtained from NASA Estimating the Circulation and Climate of the Ocean (https://www.ecco-group.org/products-ECCO-V4r4.htm). The location and area of A68a extracted from remote sensing data and the ground control points for breakup line extraction can be found in Supp. Material.

Glacier modeling code availability

Ua glacier model is available on Github (https://github.com/GHilmarG/UaSource). The code associated with glacier modeling using *Ua* is available on request from X. Wang.

References

Alley, R. B., Horgan, H. J., Joughin, I., Cuffey, K. M., Dupont, T. K., Parizek, B. R., ... & Bassis, J. (2008). A simple law for ice-shelf calving. Science, 322(5906), 1344-1344.

Arndt, J. E., Schenke, H. W., Jakobsson, M., Nitsche, F. O., Buys, G., Goleby, B., ... & Wigley, R. (2013). The International Bathymetric Chart of the Southern Ocean (IBCSO) Version 1.0—A new bathymetric compilation covering circum-Antarctic waters. Geophysical Research Letters, 40(12), 3111-3117.

Arrigo, K.R. & van Dijken, G.L., (2003). Impact of iceberg C-19 on Ross Sea primary production. Geophysical Research Letters, 30(16).

Arrigo, K.R., van Dijken, G.L., Ainley, D.G., Fahnestock, M.A., & Markus, T., (2002). Ecological impact of a large Antarctic iceberg. Geophysical Research Letters, 29(7), pp.8-1.

Benn, D.I., Warren, C.R. & Mottram, R.H., (2007). Calving processes and the dynamics of calving glaciers. Earth-Science Reviews, 82(3-4), pp.143-179.

Bouhier, N., Tournadre, J., Rémy, F., & Gourves-Cousin, R., (2018). Melting and fragmentation laws from the evolution of two large Southern Ocean icebergs estimated from satellite data. The Cryosphere, 12(7), 2267-2285.

Boy, F., Desjonquères, J. D., Picot, N., Moreau, T., & Raynal, M., (2016). CryoSat-2 SAR-mode over oceans: processing methods, global assessment, and benefits. IEEE Transactions on Geoscience and Remote Sensing, 55(1), 148-158.

Braakmann-Folgmann, A., Shepherd, A., Gerrish, L., Izzard, J., & Ridout, A. (2022). Observing the disintegration of the A68A iceberg from space. Remote Sensing of Environment, 270, 112855.

Budge, J. S., & Long, D. G. (2018). A comprehensive database for Antarctic iceberg tracking using scatterometer data. IEEE Journal of Selected Topics in Applied Earth Observations and Remote Sensing, 11(2), 434-442.

Cuffey, K.M. & Paterson, W.S.B. (2010). The Physics of Glaciers, 4th edition: Academic Press. 704.

Depoorter, M.A., Bamber, J.L., Griggs, J.A., Lenaerts, J.T., Ligtenberg, S.R., van den Broeke, M.R. & Moholdt, G., (2013). Calving fluxes and basal melt rates of Antarctic ice shelves. Nature, 502(7469), pp.89-92.

Fricker, H.A., Young, N.W., Coleman, R., Bassis, J.N. & Minster, J.B., (2005). Multi-year monitoring of rift propagation on the Amery Ice Shelf, East Antarctica. Geophysical Research Letters, 32(2).

GEBCO Bathymetric Compilation Group (2020). The GEBCO_2020 Grid – a continuous terrain model of the global oceans and land. British Oceanographic Data Centre, National Oceanography Centre, NERC, UK.

Gladstone, R.M., Bigg, G.R. & Nicholls, K.W., (2001). Iceberg trajectory modeling and meltwater injection in the Southern Ocean. Journal of Geophysical Research: Oceans, 106(C9), pp. 19903-19915.

Gudmundsson, G. H. (2008). Analytical solutions for the surface response to small amplitude perturbations in boundary data in the shallow-ice-stream approximation. The Cryosphere, 2(2), 77-93.

https://doi.org/10.5194/egusphere-2024-2790
Preprint. Discussion started: 11 November 2024

Gudmundsson, G. H. (2013). Ice-shelf buttressing and the stability of marine ice sheets. The Cryosphere, 7(2), 647-655.

Gudmundsson, G. H., Krug, J., Durand, G., Favier, L., & Gagliardini, O. (2012). The stability of grounding lines on retrograde slopes. The Cryosphere, 6(6), 1497-1505.

Han, H., Lee S., Kim, J.-I., Kim, S. H., & Kim H.C. (2019). Changes in a giant iceberg created from the collapse of the Larsen c ice shelf, Antarctic Peninsula, derived from Sentinel-1 and CryoSat-2 data." Remote Sensing 11, no. 4: 404.

Hersbach, H., Bell, B., Berrisford, P., Hirahara, S., Horanyi, A., Muñoz-Sabater, J., ... & Thepaut, J. N. (2020). The ERA5 global reanalysis. Quarterly Journal of the Royal Meteorological Society, 146(730), 1999-2049.

Hogg, A.E., & Gudmundsson, G.H. (2017). Impacts of the Larsen-C Ice Shelf calving event. Nature Climate Change 7, no. 8 (2017): 540-542.

Holland, P. R., Corr, H. F., Pritchard, H. D., Vaughan, D. G., Arthern, R. J., Jenkins, A., & Tedesco, M. (2011). The air content of Larsen ice shelf. Geophysical Research Letters, 38(10).

Huth, A., Adcroft, A., Sergienko, O., & Khan, N. (2022). Ocean currents break up a tabular iceberg. Science Advances, 8(42), eabq6974.

Jansen, D., Sandhäger, H., & Rack, W., (2005). Model experiments on large tabular iceberg evolution: ablation and strain thinning. Journal of glaciology, 51(174), pp.363-372.

Jansen, D., Schodlok, M., & Rack, W., (2007). Basal melting of A-38B: A physical model constrained by satellite observations. Remote sensing of environment, 111(2-3), pp.195-203.

Joughin, I., & MacAyeal, D.R., (2005). Calving of large tabular icebergs from ice shelf rift systems. Geophysical research letters, 32(2).

Kooyman, G.L., Ainley, D.G., Ballard, G., & Ponganis, P.J., (2007). Effects of giant icebergs on two emperor penguin colonies in the Ross Sea, Antarctica. Antarctic Science, 19(1), p.31.

Lazzara, M.A., Jezek, K.C., Scambos, T.A., MacAyeal, D.R. & Van der Veen, C.J., (1999). On the recent calving of icebergs from the Ross Ice Shelf. Polar Geography, 23(3), pp.201-212.

Long, D. G., Ballantyn, J., & Bertoia, C. (2002). Is the number of Antarctic icebergs really increasing? EOS, Transactions American Geophysical Union, 83(42), 469-474.

MacAyeal, D.R., et al, (2006). Transoceanic wave propagation links iceberg calving margins of Antarctica with storms in tropics and Northern Hemisphere. Geophysical Research Letters 33, no. 17.

McMillan, M., Shepherd, A., Sundal, A., Briggs, K., Muir, A., Ridout, A., & Wingham, D. (2014). Increased ice losses from Antarctica detected by CryoSat-2. Geophysical Research Letters, 41(11), 3899-3905.

Massom, R. A., Hill, K.L., Lytle, V.I., Worby, A.P. Paget, M.J., & Allison, I. (2001). Effects of regional fast-ice and iceberg distributions on the behaviour of the Mertz Glacier polynya, East Antarctica." Annals of Glaciology 33: 391-398.

https://doi.org/10.5194/egusphere-2024-2790
Preprint. Discussion started: 11 November 2024

Massom, R.A., Scambos, T.A., Bennetts, L.G., Reid, P., Squire, V.A. & Stammerjohn, S.E., (2018). Antarctic ice shelf disintegration triggered by sea ice loss and ocean swell. Nature, 558(7710), pp. 383-389.

McGrath, D., Steffen, K., Rajaram, H., Scambos, T., Abdalati, W. & Rignot, E., (2012). Basal crevasses on the Larsen C Ice Shelf, Antarctica: Implications for meltwater ponding and hydrofracture. Geophysical research letters, 39(16).

Merino, N., Le Sommer, J., Durand, G., Jourdain, N.C., Madec, G., Mathiot, P., & Tournadre, J., (2016). Antarctic icebergs melt over the Southern Ocean: Climatology and impact on sea ice. Ocean Modelling, 104, pp.99-110.

Nielsen, K., Stenseng, L., Andersen, O.B., & Knudsen, P. (2017). The performance & potentials of the CryoSat-2 SAR and SARIn modes for lake level estimation. Water, 9(6), 374.

Padman, L., Fricker, H. A., Coleman, R., Howard, S., & Erofeeva, L. (2002). A new tide model for the Antarctic ice shelves and seas. Annals of Glaciology, 34, 247-254.

Price, J.F., Weller, R.A., & Schudlich, R.R. (1987). Wind-driven ocean currents and Ekman transport. Science, 238(4833), 1534-1538.

Rignot, E., Casassa, G., Gogineni, P., Krabill, W., Rivera, A.U. & Thomas, R., (2004). Accelerated ice discharge from the Antarctic Peninsula following the collapse of Larsen B ice shelf. Geophysical research letters, 31(18).

Rignot, E., Jacobs, S., Mouginot, J. & Scheuchl, B., (2013). Ice-shelf melting around Antarctica. Science, 341(6143), pp.266-270.

Robinson, N.J., & Williams, M.J.M., (2012). Iceberg-induced changes to polynya operation and regional oceanography in the southern Ross Sea, Antarctica, from in situ observations. Antarctic Science, 24(5), p.514.

Russell-Head, D.S., (1980). The melting of free-drifting icebergs. Annals of glaciology, 1, pp.119-122.

Scambos, T.A., Bohlander, J.A., Shuman, C.A. & Skvarca, P., (2004). Glacier acceleration and thinning after ice shelf collapse in the Larsen B embayment, Antarctica. Geophysical Research Letters, 31(18).

Scambos, T., Sergienko, O., Sargent, A., MacAyeal, D. & Fastook, J., 2005. ICESat profiles of tabular iceberg margins and iceberg breakup at low latitudes. Geophysical Research Letters, 32(23).

Silva, T.A.M., Bigg, G.R., & Nicholls, K.W., 2006. Contribution of giant icebergs to the Southern Ocean freshwater flux. Journal of Geophysical Research: Oceans, 111(C3).

Smith, R. M., & Bigg, G. R. (2023). Impact of giant iceberg A68A on the physical conditions of the surface South Atlantic, derived using remote sensing. Geophysical Research Letters, 50(18), e2023GL104028.

Stern, A.A., Adcroft, A., & Sergienko, O. (2016). The effects of Antarctic iceberg calving-size distribution in a global climate model. Journal of Geophysical Research: Oceans, 121(8), 5773-5788.

Stuart, K.M., & Long, D.G., (2011). Tracking large tabular icebergs using the SeaWinds Ku-band microwave scatterometer. Deep Sea Research Part II: Topical Studies in Oceanography 58.11-12: 1285-1300.

Tarling, G. A., Thorpe, S. E., Henley, S. F., Burson, A., Liszka, C. M., Manno, C., ... & Abrahamsen, E. P. (2024). Collapse of a giant iceberg in a dynamic Southern

Ocean marine ecosystem: in situ observations of A-68A at South Georgia. Progress in Oceanography, 103297.
Wagner, T.J., Wadhams, P., Bates, R., Elosegui, P., Stern, A., Vella, D., Abrahamsen, E.P., Crawford, A., & Nicholls, K.W., (2014). The "footloose" mechanism: Iceberg decay from hydrostatic stresses. Geophysical Research Letters, 41(15), pp.5522-5529.
Wagner, T.J., Dell, R.W. & Eisenman, I., (2017). An analytical model of iceberg drift. Journal of Physical Oceanography, 47(7), pp.1605-1616.
Wang, X., Cheng, X., Gong, P., Shum, C.K., Holland, D.M., & Li, X., (2014). Freeboard and mass extraction of the disintegrated Mertz Ice Tongue with remote sensing and altimetry data. Remote sensing of environment 144: 1-10.
Wang, X., Holland, D.M., Cheng, X., & Gong, P., (2016). Grounding and calving cycle of Mertz Ice Tongue revealed by shallow Mertz Bank. Cryosphere 10, no. 5: 2043-2056.
Williams, G.D., Aoki, S., Jacobs, S.S., Rintoul, S.R., Tamura, T. & Bindoff, N.L., (2010). Antarctic bottom water from the Adélie and George V Land coast, East Antarctica (140–149 E). Journal of Geophysical Research: Oceans, 115(C4).
Wunsch, C., Heimbach, P., Ponte, R. M., Fukumori, I., & ECCO-GODAE CONSORTIUM MEMBERS. (2009). The global general circulation of the ocean estimated by the ECCO-Consortium. Oceanography, 22(2), 88-103.

https://doi.org/10.5194/egusphere-2024-2790
Preprint. Discussion started: 11 November 2024

Table 1. Parameters used to configure the control run of Ua glacier model.

Parameters	Setting
Iceberg Density (Considering firn layer thickness)	857 kg/m^3
Ocean Density	1028 kg/m^3
Iceberg Freeboard	32.5 m
Iceberg Draft	163.0 m
Iceberg Temperature	-20 °C
A-Glen Law	2.9377×10^{-9}
n-Glen Law	3
Surface Mass Balance	0 m/a
Basal Mass Balance	0 m/a
Ocean Drag Coefficient (Co in Ua)	$0.4\times10^{4}\ \sqrt{(\mathrm{m/s})/\mathrm{Pa}}$
m_o in Ua	0.5
U of ocean current	24.5 cm/s
V of ocean current	-3.0 cm/s
Angular Velocity	15.1°/d
Air Drag Coefficient (Ca in Ua)	$>1\times10^{10}$ (close to $+\infty$)
m_a in Ua	0.5

https://doi.org/10.5194/egusphere-2024-2790
Preprint. Discussion started: 11 November 2024

Figure 1. **(a)** to **(e)** show sequential snapshots of the major breakup events of Iceberg A68a spanning the period 2017 to 2021. The exact observation date of each of the Sentinel-1A/B images is marked in the lower left. The icebergs generated after the breakup and the main body of iceberg A68a are marked.

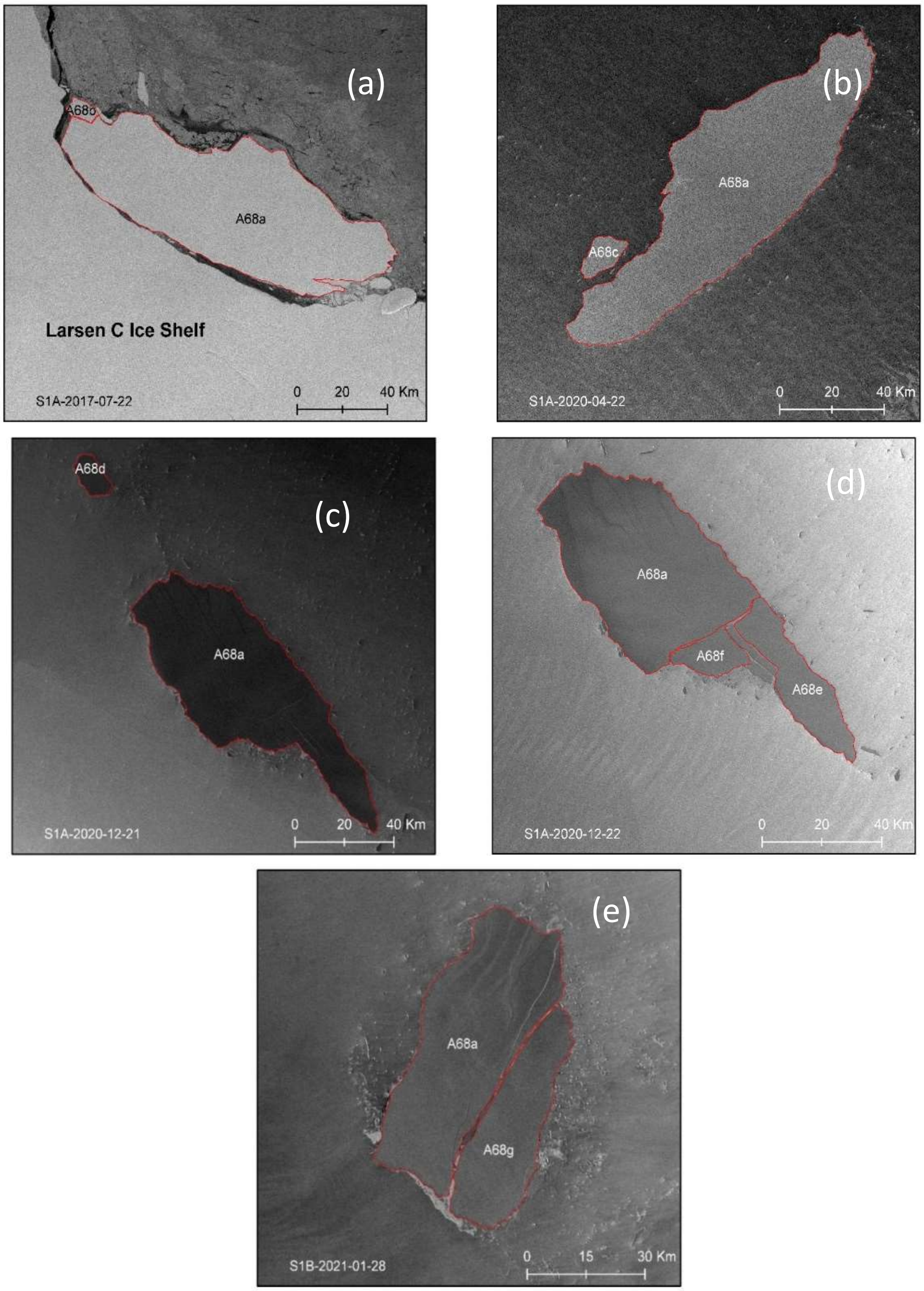

https://doi.org/10.5194/egusphere-2024-2790
Preprint. Discussion started: 11 November 2024

Figure 2. **(a)** to **(d)** shows sequential locations, outlines, breakup, and vanishing of A68a during 2021 The exact observation date of each of the MODIS images is marked in the lower left. **(e)** Location of A68a at 12:45 UTC on December 16, 2020, (MODIS). The outline of A68a is indicated with red polygon. **(f)** State of the A68a breakup at 11:50 UTC on December 17, 2020 (MODIS). The red outline is taken from **(e).**

https://doi.org/10.5194/egusphere-2024-2790
Preprint. Discussion started: 11 November 2024

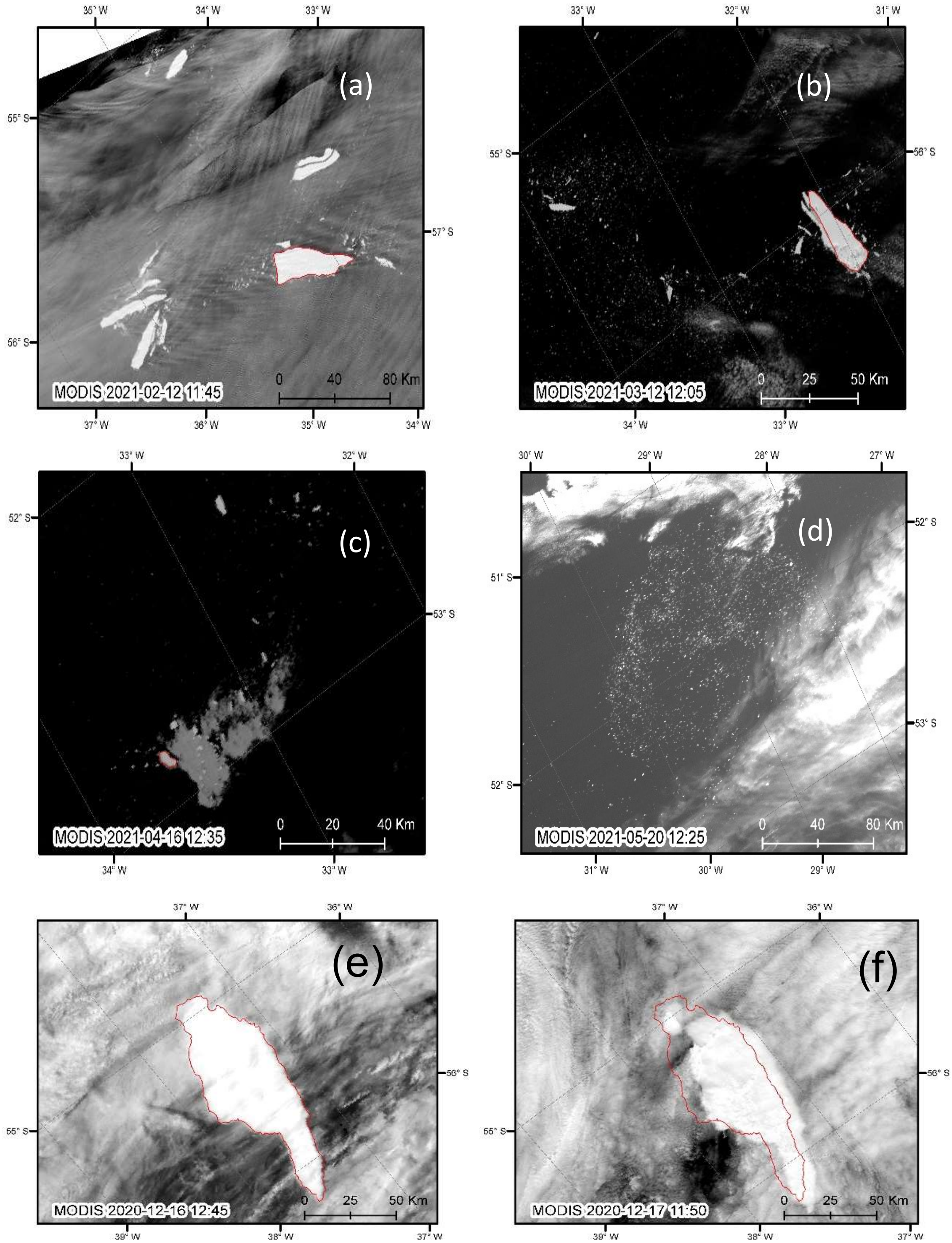

https://doi.org/10.5194/egusphere-2024-2790
Preprint. Discussion started: 11 November 2024

Figure 3. Drifting trajectory, areal changes, the major breakup, the appearance of rift lines, and the vanishing of iceberg A68a. **(a)** Drifting trajectory of A68a following its calving from Larsen C Ice Shelf in July 2017. **(b)** Outline and location of A68a before and after a breakup event in mid-December 2020. **(c)** Areal changes of A68a from calving to vanishing (left to right) as blue plus signs.

https://doi.org/10.5194/egusphere-2024-2790
Preprint. Discussion started: 11 November 2024

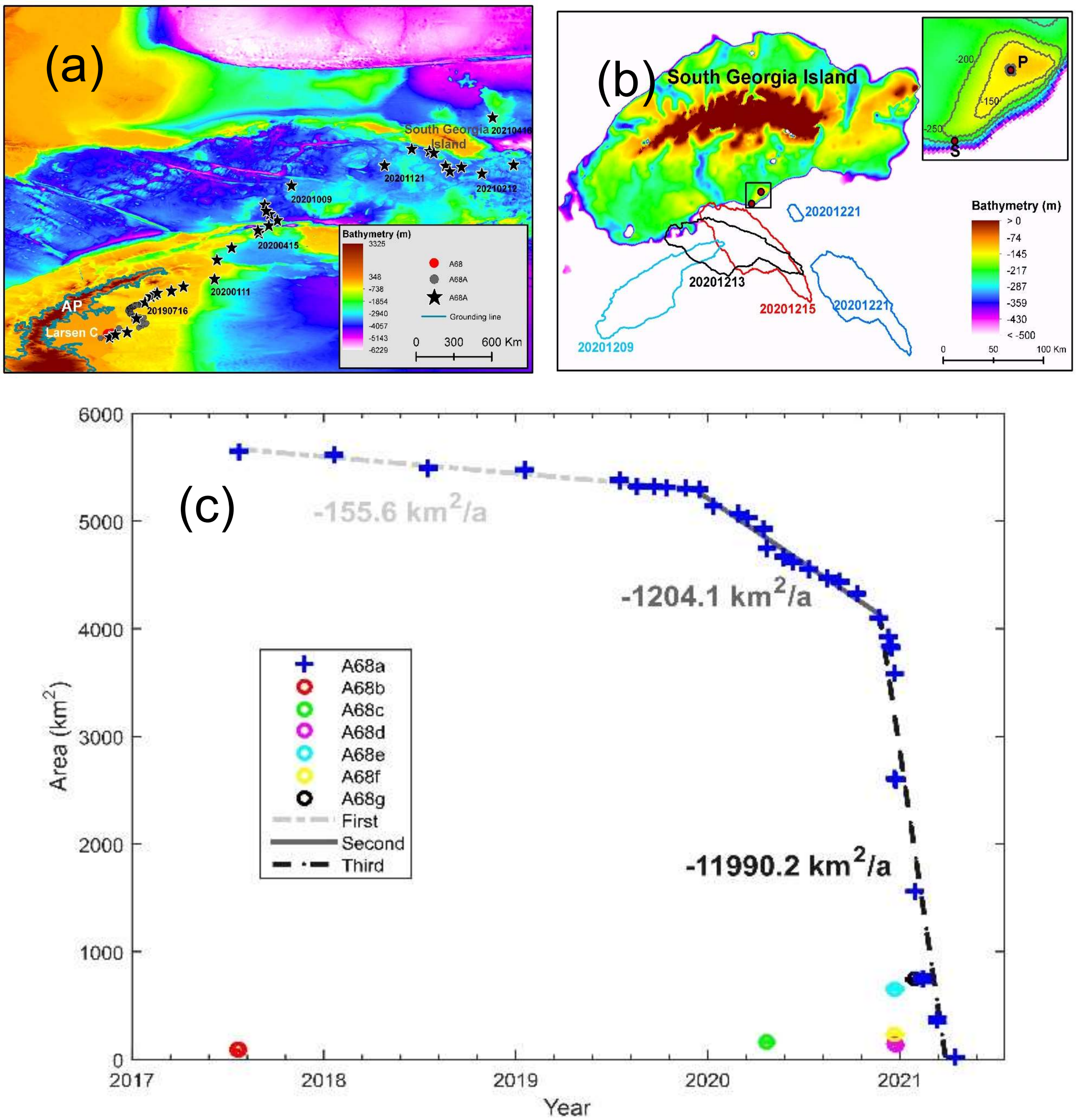

https://doi.org/10.5194/egusphere-2024-2790
Preprint. Discussion started: 11 November 2024

Figure 4. (a) ground tracks of Cryosat-2 from November 1 to December 16, 2020, in the vicinity of South Georgia Island used to extract the freeboard of iceberg A68a. The freeboard height distribution ranging from 40 m to 55 m (relative to a geoid) is indicated by blue to yellow. Yellow dots in the upper-right indicates the presence of South Georgia Island. **(b)** to **(f)** mark tracks of Cryosat-2 used in detecting iceberg A68a. The cycle, orbit, and observation date are given in the heading of each panel. Red dots indicate measurements over the surface of iceberg A68a; black dots indicate the sea surface.

https://doi.org/10.5194/egusphere-2024-2790
Preprint. Discussion started: 11 November 2024

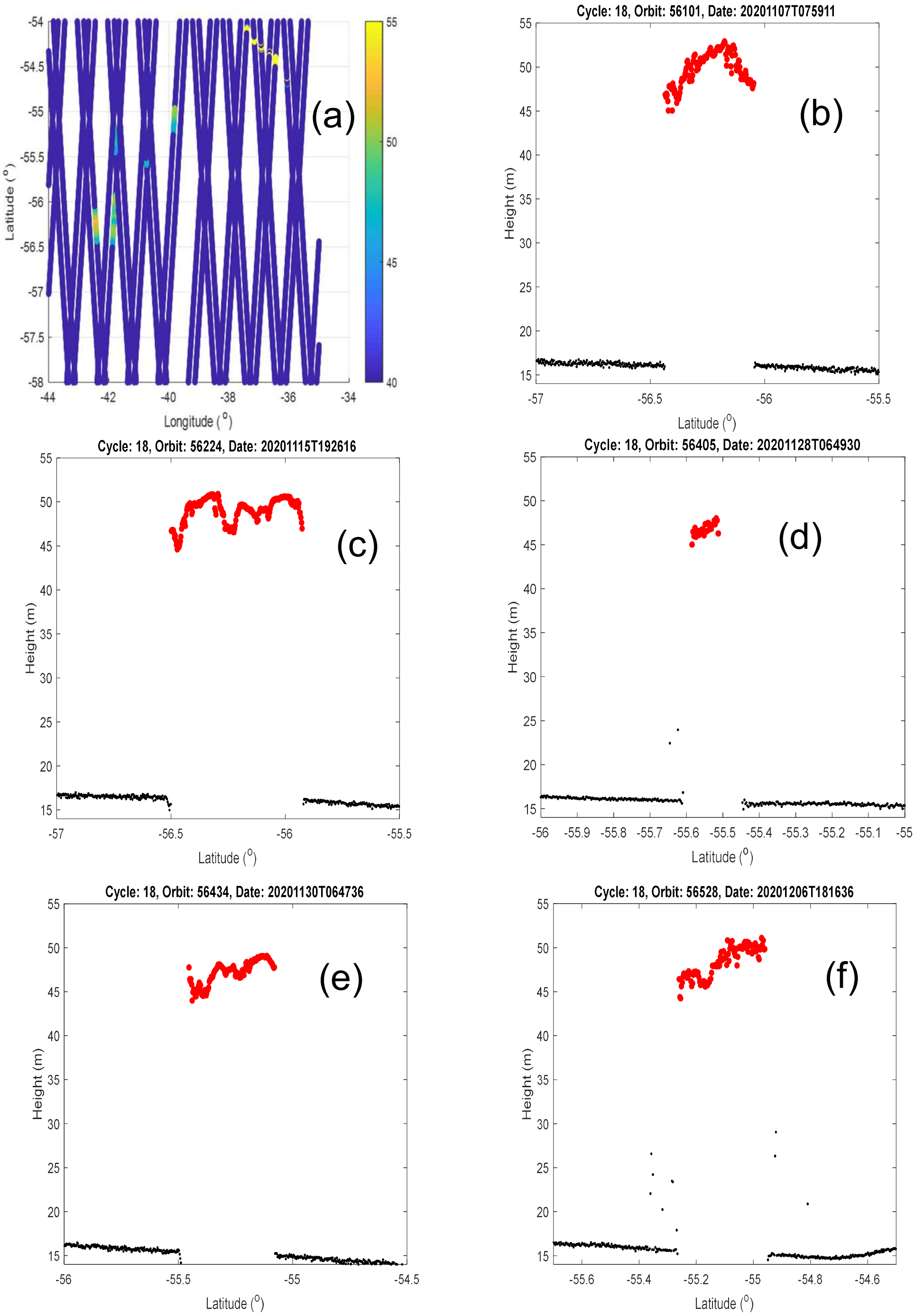

https://doi.org/10.5194/egusphere-2024-2790
Preprint. Discussion started: 11 November 2024

Figure 5. Breakup line extraction procedure. **(a)** Sentinel-1A observation on December 15, 2020, and an outline of iceberg A68a from MODIS on December 16 (red polygon). **(b)** to **(d)** show the georeferencing of Sentinel-1A observations on December 15, 21, and again 21 to the A68a location on December 16, respectively. **(e)** zoom-in of the upper part of **(d)** from which two different breakup lines are extracted.

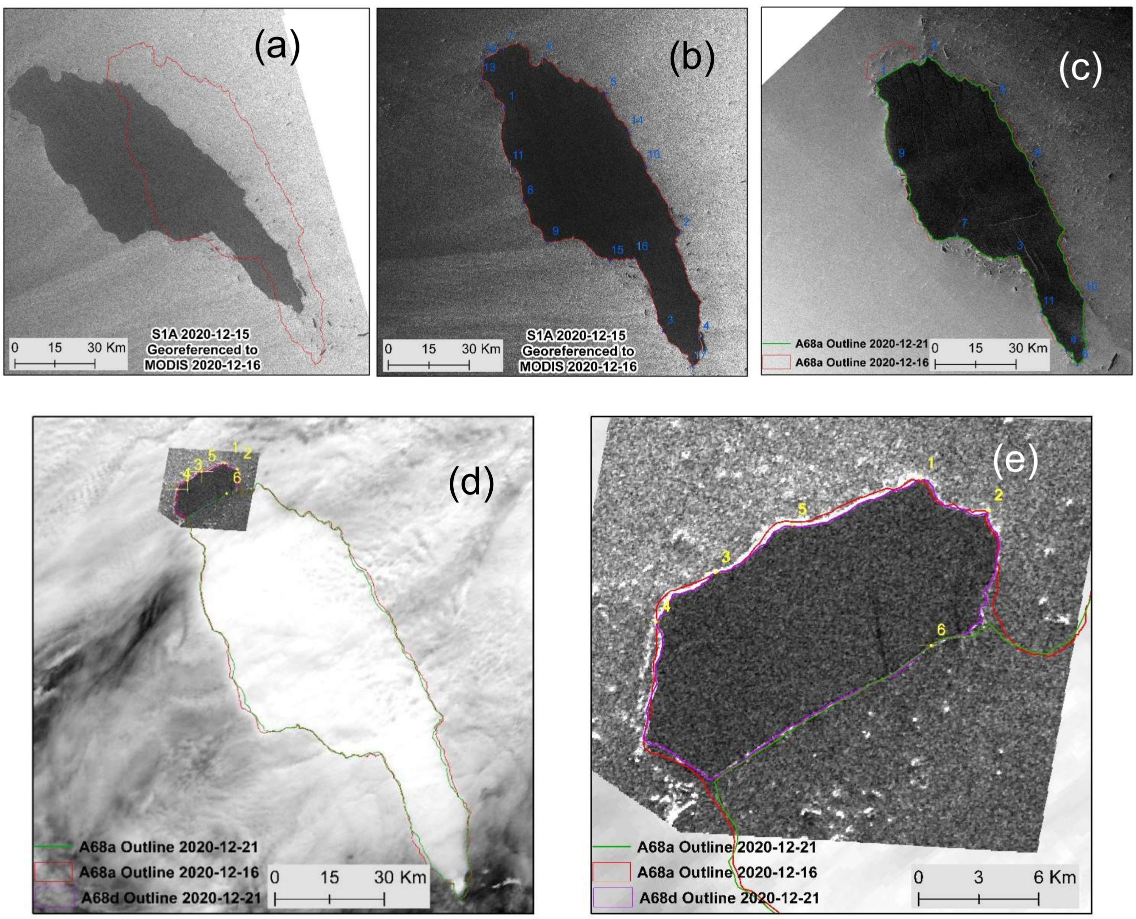

https://doi.org/10.5194/egusphere-2024-2790
Preprint. Discussion started: 11 November 2024

Figure 6. Grounding of A68a on seamount of the South Georgia Island. **(a)** Two rifts seen on December 16, 2020 (MODIS). The rift contour is extracted from Figure 5. **(b)** Grounding detection of A68a at 12:45 UTC on December 16, 2020 (MODIS). Negative values indicate grounded regions of A68a. **(c)** Zoom-in of the black box marked in **(b)**. Two rift lines are indicated with dashed curves (grey, black).

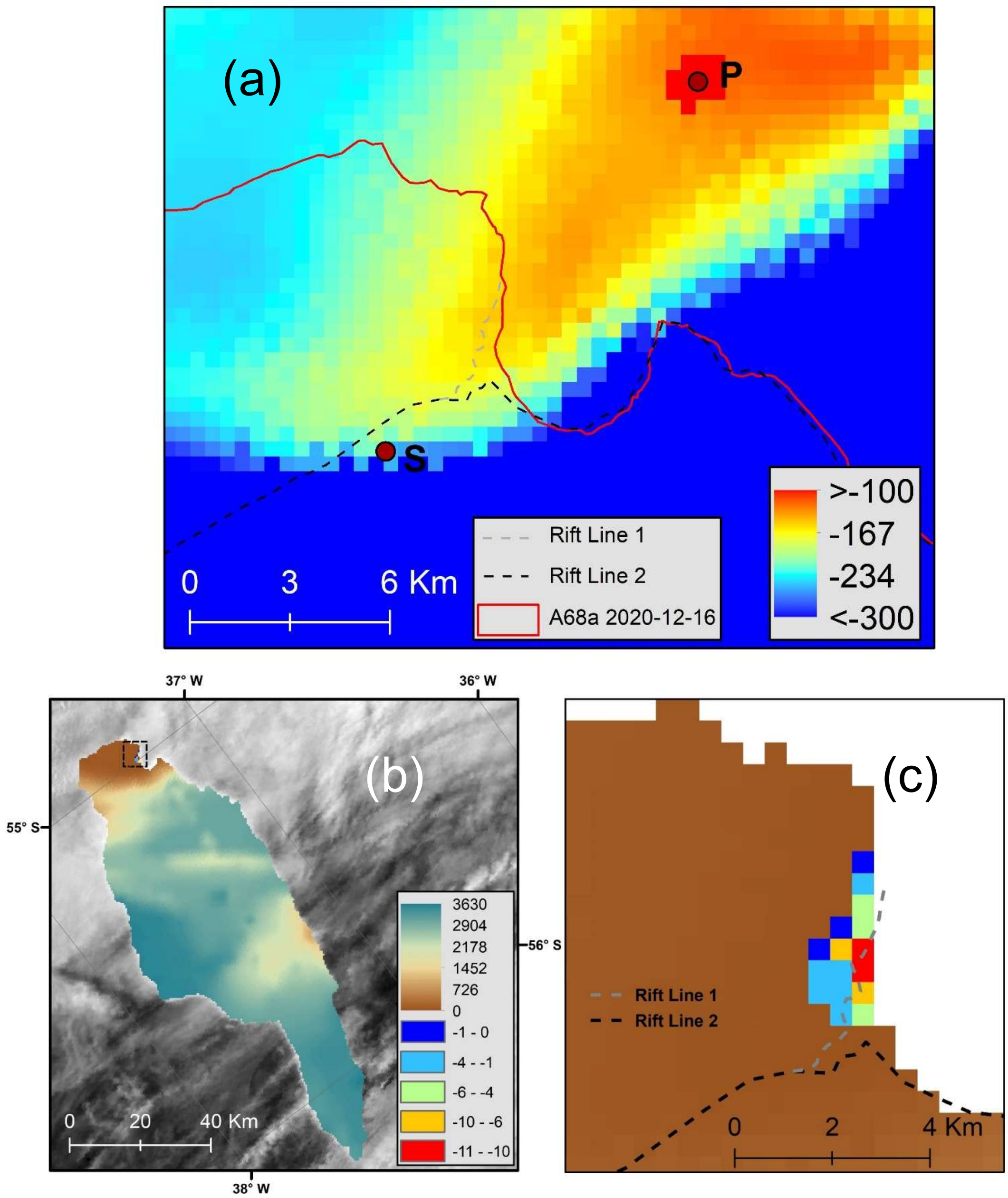

https://doi.org/10.5194/egusphere-2024-2790
Preprint. Discussion started: 11 November 2024

Figure 7. Modeling the interaction of iceberg A68a and the seafloor using Ua. **(a)** Basal ice velocity of A68a inverted from Ua, **(b)** Deviatoric stresses of A68a inverted from Ua. Red vectors are tensile; blue vectors are compressive. The maximum tensile stress is indicated with a green dot. **(c)** Zoom-in of deviatoric stresses on the grounded region of A68a. **(d)** Changes in maximum tensile stress of A68a under different settings of seafloor depth and iceberg angular velocity. Values along the x-axis stand for changes in seafloor bathymetry. U, V, and angular velocity base values are derived from remote sensing, which are equal to 24.5 cm/s, -3.0 cm/s, and 15.1 °/d, respectively. Other model parameter settings are as listed Table 1. Maximum tensile stress (black-dashed line) for zero of U and V corresponds to the small stress values as indicated by the y-axis on the right side. Stresses for other non-zero U and V correspond to the large stress values of the y-axis on the left side.

https://doi.org/10.5194/egusphere-2024-2790
Preprint. Discussion started: 11 November 2024

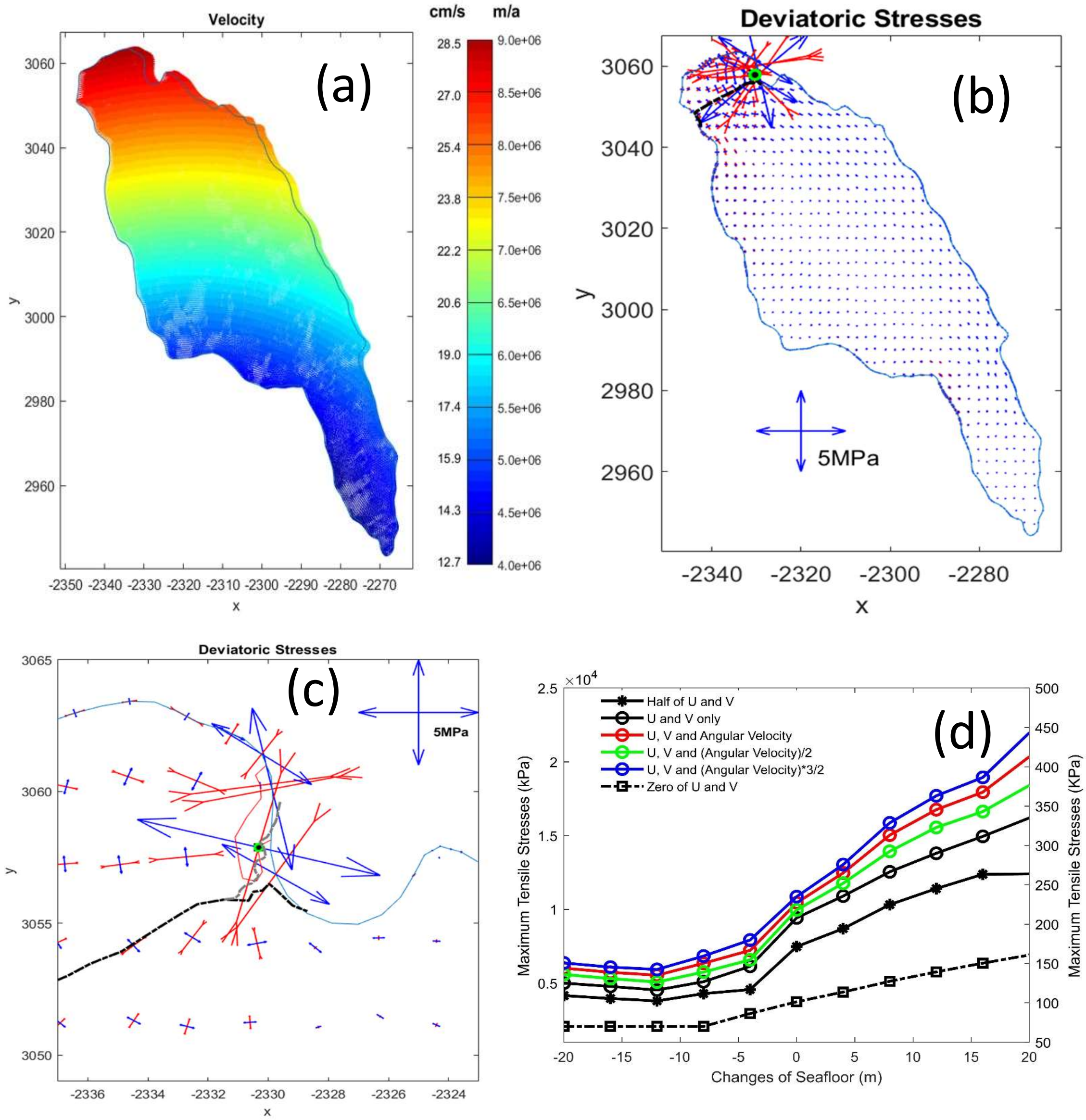

https://doi.org/10.5194/egusphere-2024-2790
Preprint. Discussion started: 11 November 2024

Figure 8. **(a)** to **(d)** basal ice velocity of A68a inverted from *Ua* when setting ocean-ice coefficient of drag Co as 0.4e5, 0.4e4, 0.4e3, and 0.4, respectively (motionless ocean). **(e)** to **(h)** corresponding deviatoric stresses of A68a inverted from *Ua* when setting Co as 0.4e5, 0.4e4, 0.4e3, and 0.4, respectively (motionless ocean). The location of maximum tensile stress is marked with a green dot. **(i)** shows the maximum tensile stress changes of A68a with Co in the still ocean. More can be found from Supplementary Material.

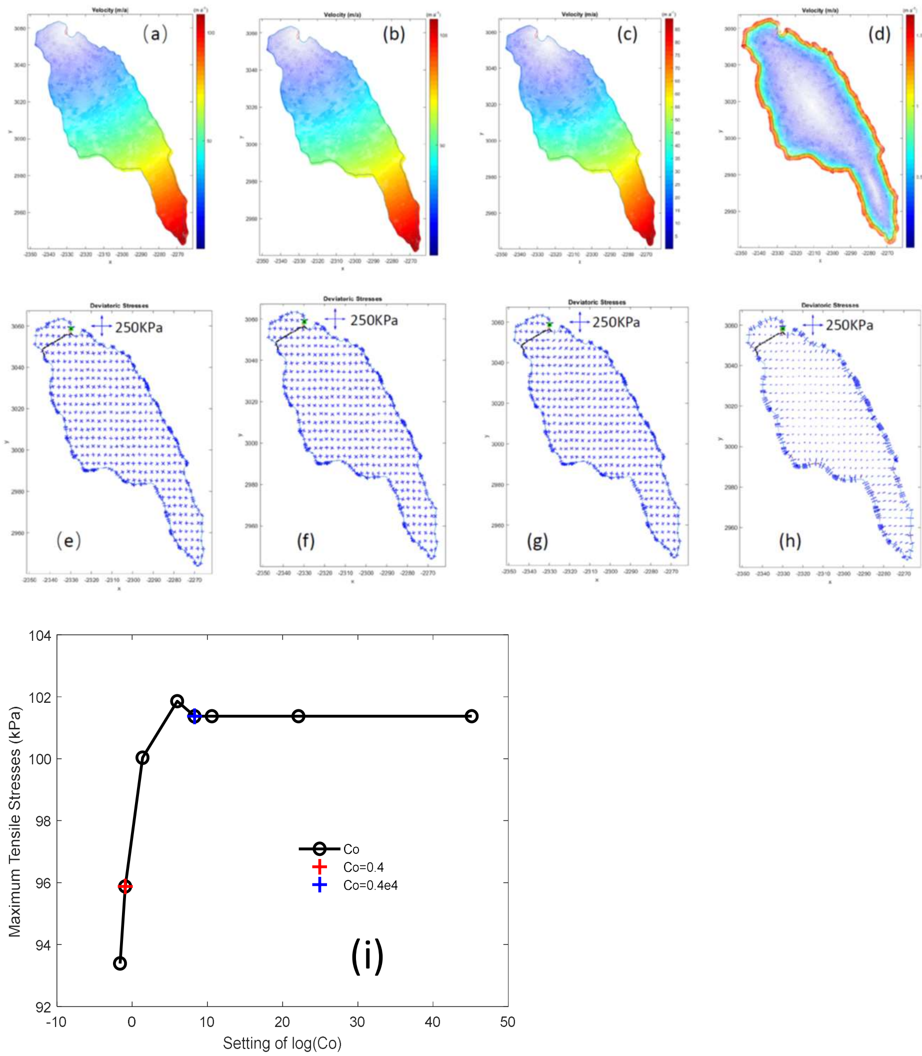

https://doi.org/10.5194/egusphere-2024-2790
Preprint. Discussion started: 11 November 2024

Figure 9. Sensitivity experiment in which the seafloor is lowered by 50 m, but other parameter settings are the same as in Extended Table 1c. **(a)** mesh grid of iceberg A68a as used in *Ua* modeling. **(b)** basal ice velocity of A68a inverted from *Ua.* **(c)** deviatoric stresses of A68a with the maximum tensile stress, marked by a green circle, showing a remarkably low value of 70 KPa.

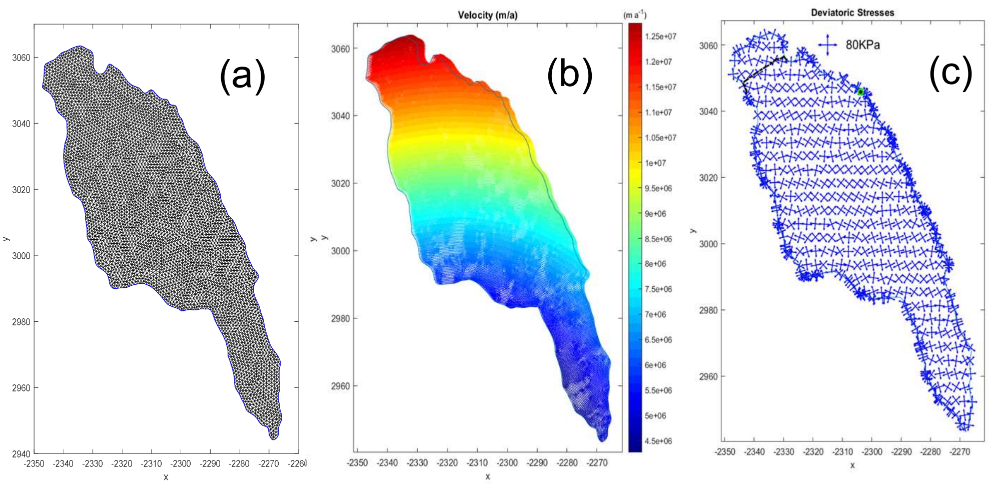

https://doi.org/10.5194/egusphere-2024-2790
Preprint. Discussion started: 11 November 2024

Figure 10. Ocean and atmosphere influences near A68a. **(a)** Historical ocean current patterns (m/s) from 1992 to 2017. **(b)** Hourly-averaged wind speed (m/s) around South Georgia Island (grey polygon). **(c)** Wind speed and direction at 13:00 UTC on December 16, 2020, during an intense polar cyclone during the time of the breakup. (ERA-5 data synchronized with MODIS observation) . **(d)** Sea-level pressure during the intense polar cyclone, 13:00 UTC, December 16, 2020. **(e)** Mean sea-level pressure change and tidal height changes in the region of A68a. **(f)** Sea surface change (m) caused by pressure change (y-axis left side) and total sea surface change (m) from tide and pressure changes (y-axis right side)..

https://doi.org/10.5194/egusphere-2024-2790
Preprint. Discussion started: 11 November 2024

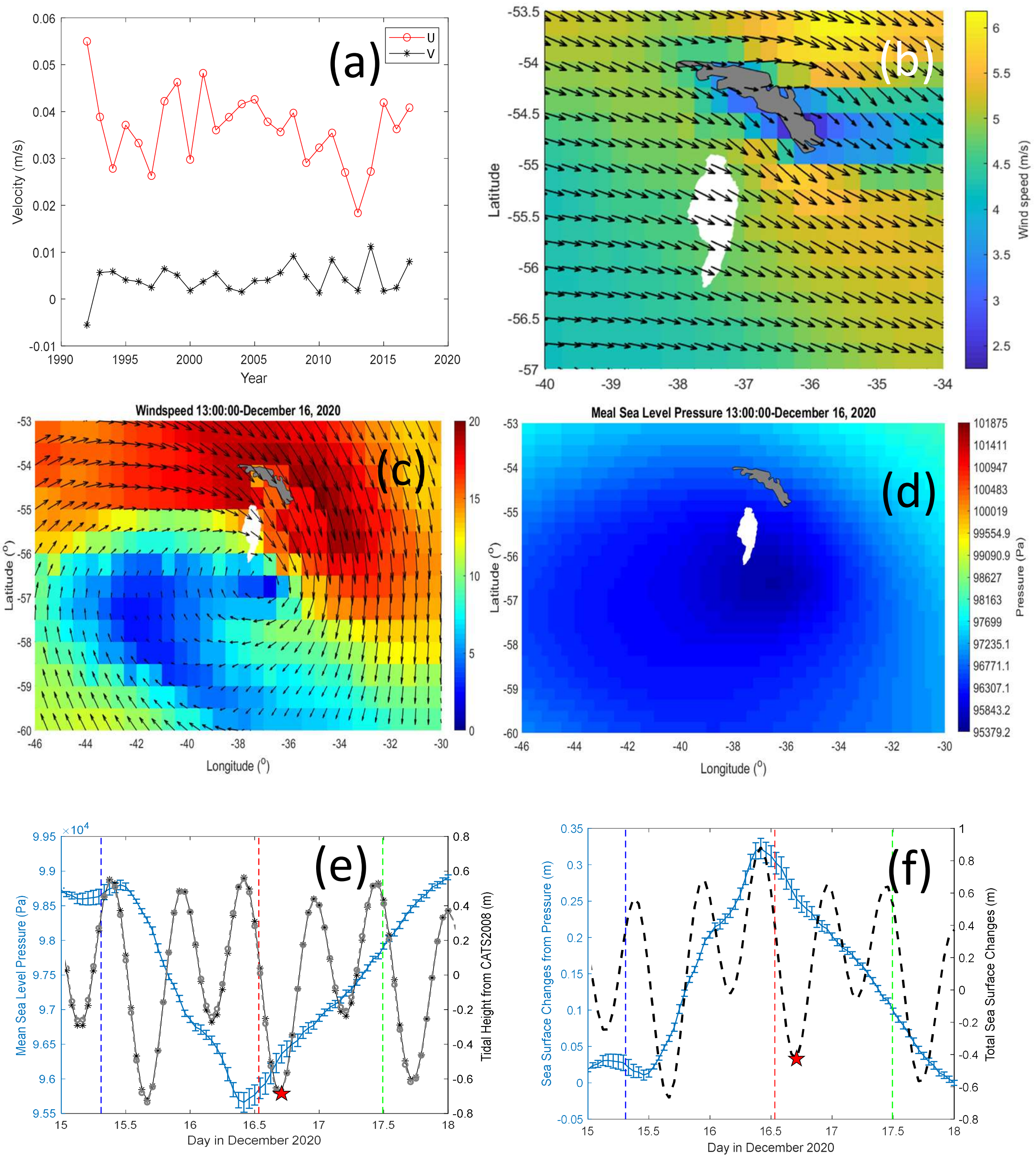

https://doi.org/10.5194/egusphere-2024-2790
Preprint. Discussion started: 11 November 2024

Competing Interests：

The authors declare that they have no conflict of interest.